The Mp*CAFA* gene encodes a ciliary protein required for spermatozoid motility in the liverwort *Marchantia polymorpha*

Mizuki Morita[1] and Katsuyuki T. Yamato[1]

[1] Faculty of Biology-Oriented Science and Technology, Kindai University, Kinokawa, Wakayama 649-6493, Japan

Corresponding author

Dr. Katsuyuki T. Yamato

E-mail: kyamato@waka.kindai.ac.jp

ORCID:

M. Morita, 0009-0005-3702-1846

K. T. Yamato, 0000-0002-7130-0911

Abstract

Bryophytes, pteridophytes and some gymnosperm species produce motile, ciliated spermatozoids that navigate themselves to the egg by regulating ciliary motility in response to a concentration gradient of attractants released from the egg and/or surrounding cells. However, the structural components of spermatozoid cilia in the land plants are largely unknown. In this study, we investigated MpCAFA (combined CAPS and FAP115; Mp1g04120) in the liverwort *Marchantia polymorpha*. The N-terminal and near C-terminal regions of MpCAFA show similarity to calcyphosine (CAPS), a mammalian EF-hand protein, and to FAP115, a ciliary protein of the green alga *Chlamydomonas reinhardtii*, respectively. Mp*CAFA* is expressed specifically in antheridia, and its orthologs are found in some algae, bryophytes, pteridophytes and cycads, but not in most of seed plants. Spermatozoids of mutants that lack functional MpCAFA exhibited significant decrease in swimming speed. Notably, these mutants showed no obvious morphological defect, including the 9+2 axoneme arrangement, and retained chemotactic capability and fertility, forming normal spores. This suggests that MpCAFA is required for spermatozoid motility but not for sperm chemotaxis or subsequent reproductive processes. Introduction of Mp$CAFA_{pro}$:Mp*CAFA-mCitrine* fully complemented the mutant phenotype and revealed MpCAFA-mCitrine was localized along the entire length of the two spermatozoid cilia. Both the CAPS-like and FAP115-like regions were essential for MpCAFA function and subcellular localization in spermatozoid, whereas the C-terminal proline-rich region was dispensable. These findings indicate that MpCAFA is a major ciliary protein in land plants and can serve as a marker to visualize spermatozoid ciliary movement.

Keywords: axoneme, bryophyte, calcyphosine, FAP115, flagella, sperm chemotaxis (4-6)

Introduction

Fertilization is the process by which an egg and a sperm fuse together to produce an offspring. Prior to fertilization, sperm detect specific chemicals released from the egg or its surrounding cells and navigates itself toward the egg. This navigation is achieved through precise regulation of ciliary movement in response to the concentration gradient of the chemical attractant. The core structure of a cilium, responsible for generating propulsion and controlling swimming direction, is the axoneme. The axoneme exhibits a conserved 9+2 arrangement of microtubules and numerous associated proteins. The structure and function of axoneme is intensively studied using animal sperm as well as the biciliate unicellular green algae *Chlamydomonas reinhardtii*. For example, sperm of the ascidian *Ciona intestinalis* makes quick turn towards the egg upon detection of the decrease of the attractant released from the egg (Shiba et al. 2008). The mechanism underlying this response involves Ca^{2+} influx triggered by the decrease in attractant, followed by modulation of cilium bending. This modulation is mediated by calaxin, which, at high Ca^{2+} concentration, binds to outer-arm dynein and inhibits microtubule sliding (Mizuno et al. 2012). The intricate structure of microtubule doublets within the *C. reinhardtii* axoneme has been elucidated by single-particle cryo-electron microscopy, revealing how flagella-associated proteins (FAPs) are integrated into the microtubule doublet assembly (Ma et al. 2019).

Motile, ciliated spermatozoids are also found in bryophytes, pteridophytes and some gymnosperms such as ginkgo and cycads. The number of spermatozoid cilium differs among land plants, from typical two in bryophytes to as many as 50,000 in the cycad *Zamia pumila* (Norstog 1986). Two cilia of a spermatozoid from liverworts and mosses are arranged in a staggered manner, the anterior and posterior cilia, while those from hornworts are oriented side-by-side (Renzaglia and Duckett 1991). In the liverwort *Marchantia polymorpha,* two cilia are reported to exhibit different beat patterns (Miyamura et al. 2018), indicating the presence of structural and functional asymmetry between the two cilia. Spermiogenesis in *M. polymorpha* is accompanied by autophagic process and drastically reorganizes the cellular components to form the characteristic elongated cell body with two cilia, two mitochondria at its ends and a plastid at its posterior end (Minamino et al. 2017; Koshimizu et al. 2022; Norizuki et al. 2022). Nevertheless, how cilium asymmetry is established during spermiogenesis, as well as its biological significance, remains to be elucidated.

The core structure of the axoneme, namely the 9+2 arrangement, is evolutionarily highly conserved among eukaryotes, including land plants. In addition, an evolutionarily conserved axonemal protein, Parkin co-regulated gene (PACRG) (Dawe et al. 2005), is encoded by the V (male) chromosome and expressed specifically in antheridia in *M. polymorpha* (Yamato et al. 2007; Higo et al. 2016), suggesting that PACRG and

possibly more proteins are conserved as ciliary proteins in *M. polymorpha* and other land plants with ciliated spermatozoids. Despite the structural conservation of axoneme, land plants have lost dynein heavy chains α, β, and γ, which are canonical components of axonemes in animals and algae (Lucas and Geisler 2022). In general, two sets of dynein complex, outer and inner dynein arms, are attached to each microtubule doublet and generate sliding forces between microtubule doublets leading to cilia beating. The outer dynein arm consists of two or three of heavy chains α, β, and γ (Inaba 2015), and thus the axoneme of land plant spermatozoids lacks outer dynein arms (Hyams and Campbell 1985). On the other hand, cilia of liverworts, hornworts and some green algae have acquired a unique protein, phosphatidylinositol-binding clathrin assembly protein-K (PICALM-K) (Minamino et al. 2023). PICALM-K is a member of AP180 N-terminal homology (ANTH) proteins that are highly conserved among eukaryotes but is distinguished from the other members by the presence of a kinase domain at its C-terminal region. PICALM-K is localized at the basal bodies and required for normal cilia function in *M. polymorpha*. These findings suggest that cilia of land plant spermatozoids have evolved through the loss and gain of their associated proteins.

In search of novel components of spermatozoid cilia, we identified and characterized MpCAFA, a novel ciliary protein, in *M. polymorpha.* MpCAFA possesses a chimeric structure, with similarity between its N- and near C-terminal regions and, respectively, mammalian calcyphosine (CAPS), an EF-hand protein, and FAP115, a ciliary protein from *C. reinhardtii*. CAPS is expressed in ciliated cells in humans (the Human Protein Atlas; Uhlén et al. 2015), although its function is unclear. FAP115 binds to the inner surface of A tubules of axoneme in *C. reinhardtii* (Ma et al. 2019) and is required for ciliary beating in the protist *Tetrahymena thermophila.* Our results demonstrate that MpCAFA localizes to spermatozoid cilia, plays a critical role in spermatozoid motility but does not affect sperm chemotaxis or fertility in *M. polymorpha*, and can serve as a tool for live imaging of cilia when fused with a fluorescent protein.

Materials and methods

Plant materials and growth conditions

Male and female accessions of *M. polymorpha*, Takaragaike-1 (Tak-1) and Takaragaike-2 (Tak-2), respectively, were used (Chiyoda et al. 2008). Plants were aseptically cultured on 1% (w/v) agar medium containing half-strength Gamborg's B5 salts (Gamborg et al. 1968), or open cultured on vermiculite soaked with 1/250 Hyponex (Hyponex Japan Co., Osaka, Japan), under continuous fluorescent light (approx. 70 μmol m^{-2} s^{-1}) at

23±1°C. Gametangiophores were induced by supplementing far-red light as previously described (Chiyoda et al. 2008).

Preparation of spermatozoids and crossing

Spermatozoids were collected by placing approx. 100 μL ultrapure water on a mature male receptacle. For crossing, freshly prepared spermatozoid suspension was applied to female receptacles of 2-3 mm in height and diameter, and again two days after the initial application. For movie recording, spermatozoid suspension collected in a microtube was kept on ice for 5 min, transferred onto a slide glass for 2 min, and then subjected to microscopic observation.

Quantitative analysis on spermatozoid motility

Movements of spermatozoids were observed under a phase-contrast microscope (BX48, Evident, Tokyo, Japan) and recorded at a resolution of 1,280 × 1,024 pixels, a rate of 100 frames per second (fps) and a shutter speed of 1/300 sec by a high-speed digital camera (HAS-U1, Ditect, Tokyo, Japan). Spermatozoids were tracked by TrackMate ver. 7.11.1 (Tinevez et al. 2017), a plugin bundled with the Fiji distribution of ImageJ, with the following modified parameters: estimated blob diameter, 30.606 pixels; initial threshold, 0.2; linking max distance, 30.606 pixels; gap-closing max distance, 30.606 pixels; gap-closing max frame gap, 2. The trajectory of each spermatozoid was generated by applying moving averages to its raw coordinates with the window size of 20. The linearity of each spermatoid trajectory was calculated as a ratio of the displacement (the linear distance between the start and end points of the trajectory) to the trajectory.

Promoter-GUS assay

The 3,084-bp Mp*CAFA* promoter region, including the 5'-UTR and 6-bp coding sequence, Mp$CAFA_{pro}$, was amplified with primers (Table S1) from Tak-1 genomic DNA by PCR and subcloned into pENTR/D-TOPO vector (Thermo Fisher Scientific, Waltham, USA). The inserted fragment was incorporated into the pMpGWB104 using Gateway LR Clonase II Enzyme mix (Thermo Fisher Scientific) (Fig. S1). To generate transgenic plants, these binary vectors were introduced germinating spores (Ishizaki et al. 2008) via *Agrobacterium tumefaciens* GV2260. Plants were soaked in GUS staining solution (5.7 mM X-Gluc (5-bromo-4-chloro-3-indolyl-β-glucuronide) (Bio Medical Science Inc., Tokyo, Japan),1.5 mM $K_3Fe(CN)_6$ (Nacalai

Tesque, Kyoto, Japan), 1.5 mM $K_4Fe(CN)_6$ (Nacalai Tesque) and 0.9% Triton X-100 (Nacalai Tesque) and incubated at 37°C overnight.

Generation of MpCAFA knock-out and complementation lines

The Mp*cafa*^{ge} lines were generated by the CRISPR/Cas9 protocol for *M. polymorpha* (Sugano et al. 2018). Two guide RNAs were designed to target the coding sequences in the third and fifth exons, sites 1 and 2, respectively (Table S1). Double stranded DNA for each gRNA was generated by annealing complementary oligonucleotides and ligated with the entry vector pMpGE_En03 digested with BsaI using DNA Ligation Kit Mighty Mix (Takara Bio Inc., Kusatsu, Japan). The gRNA expression cassette of each entry vector was transferred to the destination binary vector pMpGE010 using Gateway LR Clonase II Enzyme mix (Thermo Fisher Scientific). To generate the transgenic plants, germinating spores were infected with *A. tumefaciens* GV2260 carrying the binary vectors (Ishizaki et al. 2008).

For complementation, the Mp*CAFA* gene including its promoter region was amplified from Tak-1 genomic DNA by PCR with the primers listed in Table S1 and subcloned into the entry vector pENTR/D-TOPO (Thermo Fisher Scientific). The Mp*CAFA* gene was then transferred to the destination binary vector pMpGWB347 (Ishizaki et al. 2015) using Gateway LR Clonase II Enzyme mix (Thermo Fisher Scientific) (Fig. S1). An Mp*cafa*^{ge} plant without the CRISPR/Cas9 construct was selected from offsprings of Tak-2 × Mp*cafa*^{ge} #9-2 (Mp*cafa*^{ge} #9-2_4). To generate transgenic plants, gemmae of Mp*cafa*^{ge} #9-2_4 were infected with *A. tumefaciens* GV2260 carrying the binary vector (Tsuboyama-Tanaka and Kodama 2015).

Generation of transgenic lines expressing the MpCAFA domains separately

Coding sequence of each of the CAPS, FAP115 and FAP115+P-rich domains of Mp*CAFA* was amplified from Tak-1 genomic DNA by PCR with the primers listed in Table S1 and inserted downstream of Mp$CAFA_{pro}$ in the entry vector constructed for promoter-GUS assay described above. The expression cassettes were transferred to the pMpGWB101, pMpGWB301, pMpGWB129 and pMpGWB347 destination binary vectors (Ishizaki et al. 2015) using Gateway LR Clonase II Enzyme mix (Thermo Fisher Scientific)(Fig. S1). To generate transgenic plants, gemmae of Mp*cafa*^{ge} #9-2_4 were infected with *A. tumefaciens* GV2260 carrying the binary vectors (Tsuboyama-Tanaka and Kodama 2015).

Fluorescent microscopy

Mature antheridia were isolated from antheridiophores and observed under a fluorescence stereo microscope (MVX10, Evident) equipped with a sCMOS camera (Zyla 4.2 PLUS, Andor, Belfast, UK). Spermatozoids were stained with Kakshine (PC3)(Uno et al. 2021) to visualize nuclei and observed under an all-in-one fluorescence microscope (BZ-X810, KEYENCE, Osaka, Japan).

Electron microscopy

For TEM observation of spermatozoid cilia, mature antheridia were prefixed in 50 mM cacodylate buffer (pH7.4) containing 2% (v/v) paraformaldehyde and 2% (v/v) glutaraldehyde at 4°C overnight. The subsequent processes were carried out at Tokai Electron Microscopy, Inc. (Nagoya, Japan). The prefixed antheridia were washed three times in 50 mM cacodylate buffer at 4°C for 30 min, and then postfixed in 50 mM cacodylate buffer containing 2% (w/v) osmium tetroxide at 4°C for 3 hr. The fixed antheridia were dehydrated in an ascending series of ethanol concentrations as follows: 50% ethanol at 4°C for 30 min, 70% ethanol at 4°C 30 min, 90% at room temperature for 30 min, and 100% at room temperature for 30 min (three times) and overnight. The dehydrated antheridia were then equilibrated with propylene oxide (PO) at room temperature for 30 min (twice) and 1:1 mixture of PO and Quetol-651 (Nisshin EM Co., Tokyo, Japan) at room temperature for 3 hr, then embedded in Quetol-651 at 60°C for 48 hr. Ultra-thin sections (80-nm thick) were cut with a diamond knife using an ultramicrotome (Leica Ultracut UCT, Vienna, Austria), mounted on copper grids, stained with 2% (w/v) uranyl acetate at room temperature for 15 min and with lead stain solution (Sigma-Aldrich, St. Louis, USA) at room temperature for 3 min. The stained grids were imaged with a transmission electron microscope (JEM-1400Plus, JEOL Ltd., Tokyo, Japan) operating at 100 kV equipped with a CCD camera (EM-14830RUBY2, JEOL Ltd.).

Phylogenetic analysis

Amino acid sequences of MpCAFA and its homologs were collected from the public databases (Table S2) and aligned to construct phylogenetic trees by the MUSCLE algorithm implemented on the phylogenetic analysis software, MEGA 11 (Kumar et al. 2018; Stecher et al. 2020). The CAPS-like and FAP115-like domains were used separately to construct phylogenetic trees of the CAPS and FAP115 homologs, respectively.

Results

CAFA is conserved among streptophytes having motile spermatozoids or ciliated cells

To identify novel components of spermatozoid cilia, we searched for genes predominantly or specifically expressed in antheridium using the *Marchantia* reference genome ver. 3.1 (Bowman et al. 2017) and RNA-seq data (Higo et al. 2016), and identified Mapoly0005s0195 (currently Mp1g04120, the genome ver. 7.1), which encodes a protein with an EF-hand Ca^{2+}-binding domain. The N- and C-terminal regions of the protein showed similarity to calcyphosine (CAPS), a human EF-hand protein (47%), and to FAP115, a ciliary protein of the green alga *C. reinhardtii* (49%), respectively (Fig. 1), and thus we refer to it as MpCAFA. The FAP115-like domain was followed by a proline-rich domain (PRD) which was found only in *M. polymorpha*, *M. paleacea* and *Riccia fluitans* among the species investigated in this study, implying that the domain was acquired in the Marchantiales lineage (Table 1). While the human CAPS, its closely related proteins, calcyphosine 2 (CAPS2) and calcyphosine-like (CAPSL), and *C. reinhardtii* FAP115 have multiple conserved EF-hands, only one within the CAPS-like domain was detected in MpCAFA (represented by asterisks in Fig. 1). Phylogenetic analysis revealed that the CAPS domain of MpCAFA belongs to the CAPS2 clade, and its homologs were not detected in angiosperm genomes (Fig. 2a). FAP115 is conserved in ciliates and green algae with ciliary cells (Fig. 2b).

Homologs of MpCAFA, defined by the contiguous presence of both CAPS and FAP115 domains were found only in liverworts, mosses, pteridophytes, cycad, and charophytes, excluding the conjugating green algae (Zygnematophyceae)(Table 1; Figs. 2 and 3). Despite both ginkgo and cycads employing spermatozoids for fertilization, CAFA was identified in the *Cycas panzhihuaensis* genome but not in ginkgo, suggesting CAFA was lost in ginkgo after divergence from cycads. The concurrent absence of CAFA and cilia in Zygnematophyceae suggests a potential functional link between CAFA and cilia development or movement. Conversely, ciliated Chlorophyta, such as *C. reinhardtii*, as well as some ciliates, possess separate CAPS- and FAP115-like proteins (Table 1), reinforcing the hypothesis that these domains are associated with ciliary functions.

MpCAFA is specifically expressed in antheridia

Mp*CAFA* was identified *in silico* as one of the genes predominantly expressed in antheridia, as mentioned above. To verify its promoter activity *in planta*, transgenic lines expressing the β-glucuronidase gene (GUS) under the control of the Mp*CAFA* promoter (Mp$CAFA_{pro}$:*GUS*) were generated. Consistent with publicly available RNA-seq data (MarpolBase Expression; https://mbex.marchantia.info/chroexp/Mp1g04120/), GUS activity was detected specifically in antheridia (Fig. 4).

MpCAFA is required for proper spermatozoid motility but not for fertility

To characterize the function of MpCAFA, its loss-of-function mutants, Mp*cafa*^{ge}, were generated by CRISPR/Cas9-mediated genome editing (Sugano et al. 2018). Two target sites within the CAPS-like domain were selected (Fig. 5a), and three independent Mp*cafa*^{ge} plants were obtained for each site and sex (Figs. 5bc and S2). None of the Mp*cafa*^{ge} plants investigated showed obvious growth or morphological defects in thalli and receptacles (Fig. S3). Given the antheridium-specific expression of Mp*CAFA*, suggesting its role in spermatozoid development and/or function, we investigated spermatozoids of Mp*cafa*^{ge} plants. Morphologically normal spermatozoids were released from all male Mp*cafa*^{ge} plants upon the application of water to their receptacles (Fig. 6ab), and the cilia of spermatozoids from Mp*cafa*^{ge} retained the typical 9+2 arrangement (Fig. 6cd), indicating that MpCAFA is not essential for normal spermatozoid development. However, most of Mp*cafa*^{ge} spermatozoids displayed reduced motility compared to wild-type, with some exhibiting aberrant swimming behavior, such as circling (Movies S1-S3). To further investigate the motility defect, the trajectory of individual wild-type and Mp*cafa*^{ge} spermatozoids was tracked and analyzed (Fig. 7a). While the swimming direction of most wild-type spermatozoids was predominantly straight, Mp*cafa*^{ge} spermatozoids frequently exhibited circular trajectories or increased swing width (Fig. 7a). We examined two aspects of spermatozoid swimming behavior: swimming speed and linearity (see Materials and Methods). Average swimming speed of spermatozoids was significantly decreased in Mp*cafa*^{ge} plants, and a group of Mp*cafa*^{ge} spermatozoids showed particularly low motility, which was not found in wild-type spermatozoids (Fig. 7b). Mp*cafa*^{ge} spermatozoids also showed less straight swimming trajectories than wild-type spermatozoids (Fig. 7c). These observations suggest that MpCAFA is required for proper ciliary beating to generate propulsion and orient swim direction.

Since it is essential for spermatozoids to navigate themselves to eggs to achieve fertilization, we investigated if MpCAFA is required for the chemotactic behavior of spermatozoids. Wild-type archegonia were excised from a female receptacle and placed with wild-type or Mp*cafa*^{ge} spermatozoids in the water. Under the natural conditions, spermatozoids are attracted by unidentified substance released from the opening at the end of an archegonium, enter it, and swim through its neck to reach an egg which resides in the base of the archegonium and most likely the source of the spermatozoid attractant. However, when an archegonium excised from a female receptacle was used, spermatozoids were attracted by its base far more strongly than by the tip of its neck (Fig. 8, top), probably because the attractant is released from the wound at the base. Mp*cafa*^{ge} spermatozoids exhibited impaired motility but were strongly attracted to archegonia (Fig. 8, top), suggesting

that MpCAFA is dispensable for spermatozoid chemotactic behavior. We next tested if the Mp*cafa*^{ge} spermatozoids were fertile by applying them to wild-type female archegoniophores. All the female plants crossed with spermatozoids from Mp*cafa*^{ge} lines produced spores (Fig. 8, bottom), indicating that MpCAFA is not essential for fertility.

The above results indicate that MpCAFA is not essential for chemotaxis, fertilization, sporophyte development and sporogenesis, but for spermatozoid motility, probably for ciliary functionality.

MpCAFA is localized along the entire length of both cilia of spermatozoid

To investigate subcellular localization of the MpCAFA protein in spermatozoid, MpCAFA was fused with mCitrine at its C-terminus (Mp*CAFA*$_{pro}$:Mp*CAFA-mCitrine*), and the construct was introduced into Mp*cafa*^{ge} plants. Spermatozoids from the obtained plants showed swimming speed and linearity similar to those from Tak-1 (Fig. 7; Movie S5), indicating that Mp*CAFA*$_{pro}$:Mp*CAFA-mCitrine* functionally complemented the mutant phenotype of Mp*cafa*^{ge}. The mCitrine signal was detected in antheridia in all developmental stages (Fig. 9a) and along the entire length of both cilia of spermatozoids from the plants complemented with Mp*CAFA*$_{pro}$:Mp*CAFA-mCitrine* (Fig. 9b), indicating that MpCAFA is one of the ciliary components. The mCitrine signal at the basal ends of two cilia revealed the staggered arrangement of the anterior and posterior cilia (Fig. 9c), which also exhibits that MpCAFA is localized in axoneme.

Both CAPS- and FAP115-like regions are required for ciliary localization and function of MpCAFA

MpCAFA consists of three distinct domains: the CAPS-like, FAP115-like and proline-rich domains (Fig. 1). To investigate the contribution of each domain to ciliary function and localization, a series of constructs were prepared and expressed in Mp*cafa*^{ge} plants (Fig. S1). CAPS-FAP115-mCitrine, which lacks the proline-rich domain, recovered swimming speed (Fig. 10), revealing that the proline-rich domain is dispensable for the MpCAFA functionality. On the other hand, none of the constructs with CAPS-like or FAP115-like domain alone (CAPS, CAPS-mCitrine, FAP115, and FAP115-mCitrine), regardless of mCitrine-tagging, could complement the Mp*cafa*^{ge} phenotype (Fig. 10), suggesting that both regions are required for the MpCAFA functionality.

Previous studies have localized mammalian CAPS (Setu et al. 2024) and algal FAP115 (Ma et al. 2019) to cilia, suggesting that the CAPS- or FAP115-like domains within MpCAFA may independently target cilia. To investigate this, we examined the subcellular localization of mCitrine-tagged proteins carrying these

domains separately. Full-length MpCAFA-mCitrine and a truncated protein lacking the proline-rich domain (CAPS-FAP115-mCitrine) were consistently detected in antheridia of all developmental stages and along the entire length of cilia (Fig. 9), indicating that the proline rich domain is dispensable for ciliary localization. In contrast, CAPS-mCitrine (carrying only the CAPS-like domain) was detected in antheridia prior to maturation but was absent from mature antheridia and spermatozoids (Fig. 9). FAP115-mCitrine (carrying only the FAP115-like domain) exhibited weak expression in immature antheridia, localized near the periphery of the male receptacle (Fig. 9a), and was detected at the anterior end of the nucleus in spermatozoid (Fig. 9b). These findings suggest that both the CAPS- and FAP115-like domains are required for proper ciliary localization and/or stability of MpCAFA.

Discussion

Intracellular Ca^{2+} concentration plays a critical role in regulating ciliary movement and sperm chemotaxis in animals. However, the molecular mechanisms of Ca^{2+} signaling during sperm chemotaxis in land plants remain largely unexplored. Although the *P. patens* non-selective Ca^{2+} channel GLR has been shown to function in both sperm chemotaxis and sporophyte development (Ortiz-Ramírez et al. 2017), comprehensive understanding is lacking. In this study, we analyzed the function of Mp*CAFA*, a gene encoding an EF-hand domain protein involved in Ca^{2+} binding, in sperm chemotaxis.

MpCAFA is unique in possessing contiguous CAPS and FAP115 domains in a single polypeptide. Although the biological significance of this structure is unknown, homologs of MpCAFA are conserved among charophytes, bryophytes, pteridophytes and gymnosperm cycad, whereas they are expressed as distinct proteins in ciliated chlorophytes and ciliates (Figs. 1 and 2; Table 1). The charophyte conjugating algae, including *Mesotaenium endlicherianum* and *Spirogloea muscicola,* have undergone a secondary loss of spermatozoids, which is associated with the concurrent loss of CAFA. This correlation is also evident in seed plants: *C. panzhihuaensis*, gymnosperm, have both spermatozoids and CAFA, while angiosperms lack both. Although an intact copy of *CAFA* has not been identified in the genome of *Ginkgo biloba* (Fig. S4), a gymnosperm that produces spermatozoids, the overall trend supports the conclusion that CAFA is a structural and functional component of cilia.

To elucidate the function of MpCAFA in sperm chemotaxis of *M. polymorpha*, we generated genome-edited plants by CRISPR/Cas9. Loss of the Mp*CAFA* function led to a significant reduction in spermatozoid motility (Fig. 7). However, Mp*cafa*^{ge} spermatozoids retained not only normal morphology,

including the canonical 9+2 microtubule structure of the axoneme, but also chemotactic behavior and fertility. Expression of MpCAFA-mCitrine complemented the impaired spermatozoid motility in Mp*cafa*^{ge} and demonstrated uniform distribution of MpCAFA along the entire length of both cilia (Fig. 9b). These results suggest that MpCAFA is one of structural components of the axoneme and plays a role in propagation of ciliary oscillation from the basal region to the distal end, but not in chemotactic behavior and fertility.

Studies on ciliary fine structure have been mainly conducted in ciliate *Tetrahymena thermophila* and green alga *C. reinhardtii*. Recently, localization of microtubule inner proteins (MIPs) has been investigated with cryogenic electron microscopy (cryo-EM), revealing MIPs interact with tubulin. One of MIPs, RIB72, the 72-kDa ribbon-associated protein containing an EF-hand domain, binds to microtubules and localizes within the A-tubule of ciliary microtubule doublets, contributing to ciliary beat frequency in *T. thermophila* (Stoddard et al. 2018). Interestingly, in *T. thermophila,* proteomic analysis of cilia of *rib72a/b* null mutants revealed a decrease in ciliary CAPS and FAP115 (Fabritius et al. 2021), and the mutants showed abnormal bend during the power stroke, suggesting the structural integrity of cilia was compromised in the mutants due to the lack of these proteins (Stoddard et al. 2018). Similarly, the reduced propagation of ciliary oscillation and speed in the Mp*cafa*^{ge} spermatozoids could be explained by decreased ciliary rigidity due to the loss of functional MpCAFA. In *T. thermophila*, FAP115 localizes to cilia and basal bodies, and its null mutant showed decreased ciliary beat frequency and swimming speed, despite cilium bend during the power stroke was not discernibly affected (Fabritius et al. 2021). In *C. reinhardtii*, RIB72 and FAP115 have also been shown to localize within the A-tubule (Ma et al. 2019), although their functions remain unclear. These findings demonstrate that CAPS and FAP115, as well as CAFA, are components of the axoneme assembly and are involved in ciliary movement.

MpCAFA consists of CAPS, FAP115 and P-rich domains. To investigate the function of each domain, truncated proteins were expressed in Mp*cafa*^{ge} plants. The P-rich domain is conserved among liverworts, but its elimination did not largely affect the function of MpCAFA, suggesting its dispensable nature. The CAPS and FAP115 domains, in contrast, were both required for proper allocation of MpCAFA to cilia. CAPS-mCitrine was abundantly present in younger antheridia but not detected in mature antheridia and spermatozoids, suggesting autophagic degradation during spermiogenesis. Unlike CAPS-mCitrine, FAP115-mCitrine was detected in spermatozoids, but its localization was altered to the posterior region of the spermatozoid, where a plastid and the posterior mitochondrion are present. These observations implies that the CAPS and FAP115 domains play a role in ciliary localization and stability of MpCAFA during spermiogenesis, respectively. In *T. thermophila,* RIB72 recruits FAP115, probably also CAPS, to axoneme (Fabritius et al.

2021). *M. polymorpha* also has the RIB72 ortholog (Mp8g05900) expressed specifically in antheridia (MarpolBase Expression; Kawamura et al. 2022), but the FAP115 domain alone was not incorporated into cilia. It is not clear if CAPS plays a role in ciliary localization of FAP115 in animals, but the CAPS domain may be required for proper localization of MpCAFA in *M. polymorpha*, suggesting a similar function in animal spermiogenesis.

In this study, we identified MpCAFA, a protein that functions in spermatozoid motility. Our results demonstrated that both CAPS and FAP115 domains are indispensable for normal ciliary function in *M. polymorpha*. Despite being conserved across a wide variety of eukaryotes, CAPS and its homologs in animals have received limited attention compared to FAP115. Our findings on MpCAFA should shed light on the function of CAPS and its homologs in organisms other than *M. polymorpha*. Simultaneously, further investigation is required to understand the biological significance of the conserved chimeric structure of CAFA. Finally, being abundantly present in both cilia, MpCAFA can be used as a ciliary marker that does not affect spermatozoid development, swimming and fertility.

Acknowledgments

We thank Dr. Kazuo Yamagata (Kindai University) for recording and providing the fluorescent microscopy movie (Movie S6) used in this study. We thank Drs. Naoki Minamino (Fukuoka University) and Takashi Ueda (National Institute of Basic Biology) for insightful discussion. We also thank Dr. Katsura Zaitsu (Kindai University) for advice in coding R scripts. This work was supported in part by JSPS KAKENHI Grant Numbers 24112715 and 21K06237, Japanese Association for Marine Biology (JAMBIO) (No. 35) and the Project Research of the Faculty of Biology-Oriented Science and Technology, Kindai University, 2022-2024 (No. 21-I-2) to K.T.Y.

Statements and Declarations

The authors declare that they have no conflict of interest.

References

Bowman JL, Kohchi T, Yamato KT, et al (2017) Insights into Land Plant Evolution Garnered from the *Marchantia polymorpha* Genome. Cell 171:287-304.e15. https://doi.org/10.1016/j.cell.2017.09.030

Chiyoda S, Ishizaki K, Kataoka H, et al (2008) Direct transformation of the liverwort *Marchantia polymorpha* L. by particle bombardment using immature thalli developing from spores. Plant Cell Reports 27:1467–1473. https://doi.org/10.1007/s00299-008-0570-5

Dawe HR, Farr H, Portman N, et al (2005) The Parkin co-regulated gene product, PACRG, is an evolutionarily conserved axonemal protein that functions in outer-doublet microtubule morphogenesis. Journal of Cell Science 118:5421–5430. https://doi.org/10.1242/jcs.02659

Fabritius AS, Bayless BA, Li S, et al (2021) Proteomic analysis of microtubule inner proteins (MIPs) in Rib72 null *Tetrahymena* cells reveals functional MIPs. Molecular Biology of the Cell 32:. https://doi.org/10.1091/mbc.E20-12-0786

Gamborg OL, Miller RA, Ojima K (1968) Nutrient requirements of suspension cultures of soybean root cells. Experimental Cell Research 50:151–158. https://doi.org/10.1016/0014-4827(68)90403-5

Higo A, Niwa M, Yamato KT, et al (2016) Transcriptional Framework of Male Gametogenesis in the Liverwort *Marchantia polymorpha* L. Plant Cell Physiol 57:325–338. https://doi.org/10.1093/pcp/pcw005

Hyams JS, Campbell CJ (1985) Widespread absence of outer dynein arms in the spermatozoids of lower plants. Cell Biology International Reports 9:841–848. https://doi.org/10.1016/0309-1651(85)90103-1

Inaba K (2015) Calcium sensors of ciliary outer arm dynein: functions and phylogenetic considerations for eukaryotic evolution. Cilia 4:6. https://doi.org/10.1186/s13630-015-0015-z

Ishizaki K, Chiyoda S, Yamato KT, Kohchi T (2008) *Agrobacterium*-mediated transformation of the haploid liverwort *Marchantia polymorpha* L., an emerging model for plant biology. Plant and Cell Physiology 49:1084–1091. https://doi.org/10.1093/pcp/pcn085

Ishizaki K, Nishihama R, Ueda M, et al (2015) Development of gateway binary vector series with four different selection markers for the liverwort *Marchantia polymorpha*. PLoS ONE 10:. https://doi.org/10.1371/journal.pone.0138876

Koshimizu S, Minamino N, Nishiyama T, et al (2022) Phylogenetic distribution and expression pattern analyses identified a divergent basal body assembly protein involved in land plant spermatogenesis. New Phytologist 236:1182–1196. https://doi.org/10.1111/nph.18385

Kumar S, Stecher G, Li M, et al (2018) MEGA X: Molecular evolutionary genetics analysis across computing platforms. Molecular Biology and Evolution 35:1547–1549. https://doi.org/10.1093/molbev/msy096

Liu Y, Wang S, Li L, et al (2022) The *Cycas* genome and the early evolution of seed plants. Nat Plants 8:389–401. https://doi.org/10.1038/s41477-022-01129-7

Lucas J, Geisler M (2022) Sequential loss of dynein sequences precedes complete loss in land plants. Plant Physiology 189:1237–1240. https://doi.org/10.1093/plphys/kiac151

Ma M, Stoyanova M, Rademacher G, et al (2019) Structure of the Decorated Ciliary Doublet Microtubule. Cell 179:909-922.e12. https://doi.org/10.1016/j.cell.2019.09.030

Minamino N, Fujii H, Murata H, et al (2023) Analysis of Plant-Specific ANTH Domain-Containing Protein in *Marchantia polymorpha*. Plant Cell Physiol 64:1331–1342. https://doi.org/10.1093/pcp/pcad118

Minamino N, Kanazawa T, Nishihama R, et al (2017) Dynamic reorganization of the endomembrane system during spermatogenesis in *Marchantia polymorpha*. Journal of Plant Research 130:433–441. https://doi.org/10.1007/s10265-017-0909-5

Miyamura S, Nomura M, Mitsuhashi F, Nagumo T (2018) High-Speed Video Analysis of the Flagellar Movement of Isogametes during Fertilization of the Marine Green Macroalga, *Chaetomorpha spiralis* (Ulvophyceae, Chlorophyta). Cytologia 83:109–114. https://doi.org/10.1508/cytologia.83.109

Mizuno K, Shiba K, Okai M, et al (2012) Calaxin drives sperm chemotaxis by Ca^{2+}-mediated direct modulation of a dynein motor. Proc Natl Acad Sci USA 109:20497–20502. https://doi.org/10.1073/pnas.1217018109

Norizuki T, Minamino N, Sato M, et al (2022) Dynamic rearrangement and autophagic degradation of mitochondria during spermiogenesis in the liverwort *Marchantia polymorpha*. Cell Reports 39:. https://doi.org/10.1016/j.celrep.2022.110975

Norstog KJ (1986) The Blepharoplast of *Zamia pumila* L. Botanical Gazette 147:40–46

Ortiz-Ramírez C, Michard E, Simon AA, et al (2017) GLUTAMATE RECEPTOR-LIKE channels are essential for chemotaxis and reproduction in mosses. Nature 549:91–95. https://doi.org/10.1038/nature23478

Renzaglia KS, Duckett JG (1991) Towards an understanding of the differences between the blepharoplasts of mosses and liverworts, and comparisons with hornworts, biflagellate lycopods and charophytes: a numerical analysis. New Phytologist 117:187–208. https://doi.org/10.1111/j.1469-8137.1991.tb04900.x

Setu B, Nie Q, Echele G, Spencer SA (2024) Calcyphosine is a microtubule-associated protein required for spindle formation and function. 2023.12.29.573632

Shiba K, Baba SA, Inoue T, Yoshida M (2008) Ca^{2+} bursts occur around a local minimal concentration of attractant and trigger sperm chemotactic response. Proceedings of the National Academy of Sciences 105:19312–19317

Stecher G, Tamura K, Kumar S (2020) Molecular evolutionary genetics analysis (MEGA) for macOS. Molecular Biology and Evolution 37:1237–1239. https://doi.org/10.1093/molbev/msz312

Stoddard D, Zhao Y, Bayless BA, et al (2018) *Tetrahymena* RIB72A and RIB72B are microtubule inner proteins in the ciliary doublet microtubules. MBoC 29:2566–2577. https://doi.org/10.1091/mbc.E18-06-0405

Sugano SS, Nishihama R, Shirakawa M, et al (2018) Efficient CRISPR/Cas9-based genome editing and its application to conditional genetic analysis in *Marchantia polymorpha*. PLoS ONE 13:. https://doi.org/10.1371/journal.pone.0205117

Tinevez J-Y, Perry N, Schindelin J, et al (2017) TrackMate: An open and extensible platform for single-particle tracking. Methods 115:80–90. https://doi.org/10.1016/j.ymeth.2016.09.016

Tsuboyama-Tanaka S, Kodama Y (2015) AgarTrap-mediated genetic transformation using intact gemmae/gemmalings of the liverwort *Marchantia polymorpha* L. J Plant Res 128:337–344. https://doi.org/10.1007/s10265-014-0695-2

Uhlén M, Fagerberg L, Hallström BM, et al (2015) Tissue-based map of the human proteome. Science 347:1260419. https://doi.org/10.1126/science.1260419

Uno K, Sugimoto N, Sato Y (2021) N-aryl pyrido cyanine derivatives are nuclear and organelle DNA markers for two-photon and super-resolution imaging. Nature Communications 12:. https://doi.org/10.1038/s41467-021-23019-w

Yamato KT, Ishizaki K, Fujisawa M, et al (2007) Gene organization of the liverwort Y chromosome reveals distinct sex chromosome evolution in a haploid system. Proceedings of the National Academy of Sciences 104:6472–6477. https://doi.org/10.1073/pnas.0609054104

Supplementary data

Supplementary data are available online.

Tables

Table 1. Distribution of cilia and CAFA-related proteins in Viridiplantae and ciliates

		Cillia	Spermatozoid	Length (aa)	CAPS	Link	FAP115	PRD	RIB72
Angiosperm	*Arabidopsis thaliana*	-	-	-	-	-	-		-
Gymnosperm	*Cycas panzhihuaensis*	+	+	413					
Pteridophytes	*Adiantum capillus*	+	+	382					
	Ceratopteris richardii	+	+	428					
	Diphasiastrum complanatum	+	+	412					
	Selaginella moellendorffii	+	+	412					
Bryophytes	*Sphagnum magellanicum*	+	+	406					
	Physcomitrium patens	+	+	406					
	Ceratodon purpureus	+	+	406					
	Marphantia polymorpha	+	+	470					
	Marchantia paleacea	+	+	470					
	Riccia fluitans	+	+	472					
	Megaceros flagellaris	+	+	417					
	Phaeoceros carolinianus	+	+	417					
	Anthoceros agrestis	+	+	417					
Charophytes	*Chara braunii*	+	-	506					
	Klebsormidium nitens	+	-	410					
	Chlorokybus atmophyticus	+	-	260					
	Mesostigma viride	+	-	303					
	Mesotaenium endlicherianum	-	-	-	-		-		-
	Spirogloea muscicola	-	-	-	-		-		-
Chlorophytes	*Chlamydomonas reinhardtii*	+	-	456, 230					
	Gonium pectorale	+	-	324, 230					
	Volvox africanus	+	-	430, 231					
	Micromonas commoda	+	-	374, 220					
	Ostreococcus tauri	-	-	-	-		-		
ciliates	*Paramecium sonneborni*	+	-	195, 926					
	Stentor coeruleus	+	-	188, 911					
	Tetrahymena thermophila SB210	+	-	191, 1008					

PRD, Proline-rich domain.

"Link" indicates both the CAPS-like and FAP115-like domains reside within a single protein.

Sequences shown in light blue and grey boxes are truncated. Sequence accessions are listed in Table S2.

Figures

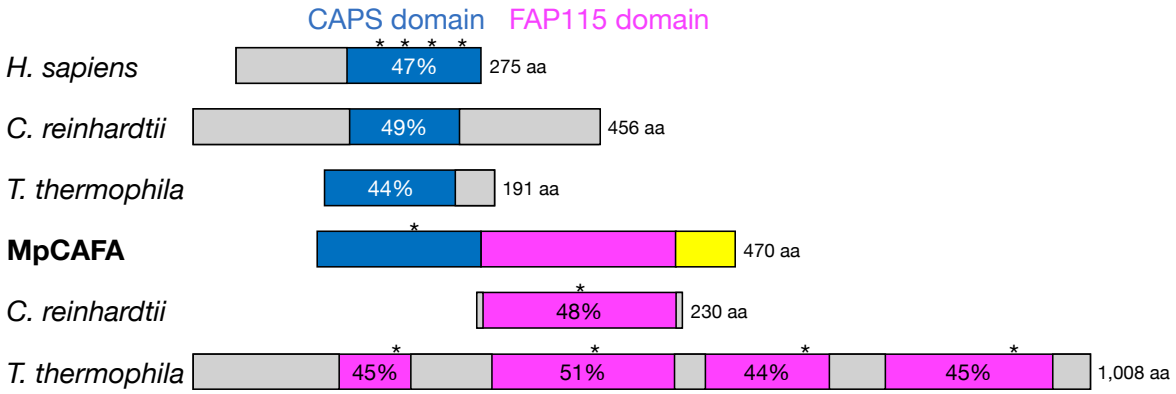

Fig. 1 MpCAFA consists of conserved CAPS- and FAP115-like domains

Schematic illustration of the structure of MpCAFA and comparison of its homologs. The CAPS-like, FAP115-like and proline-rich domains are shown in blue, magenta and yellow, respectively. Asterisks indicate locations of predicted EF-hands. The percentages in other species' domains are similarity to MpCAFA. Accessions of above sequences are given in Table S2.

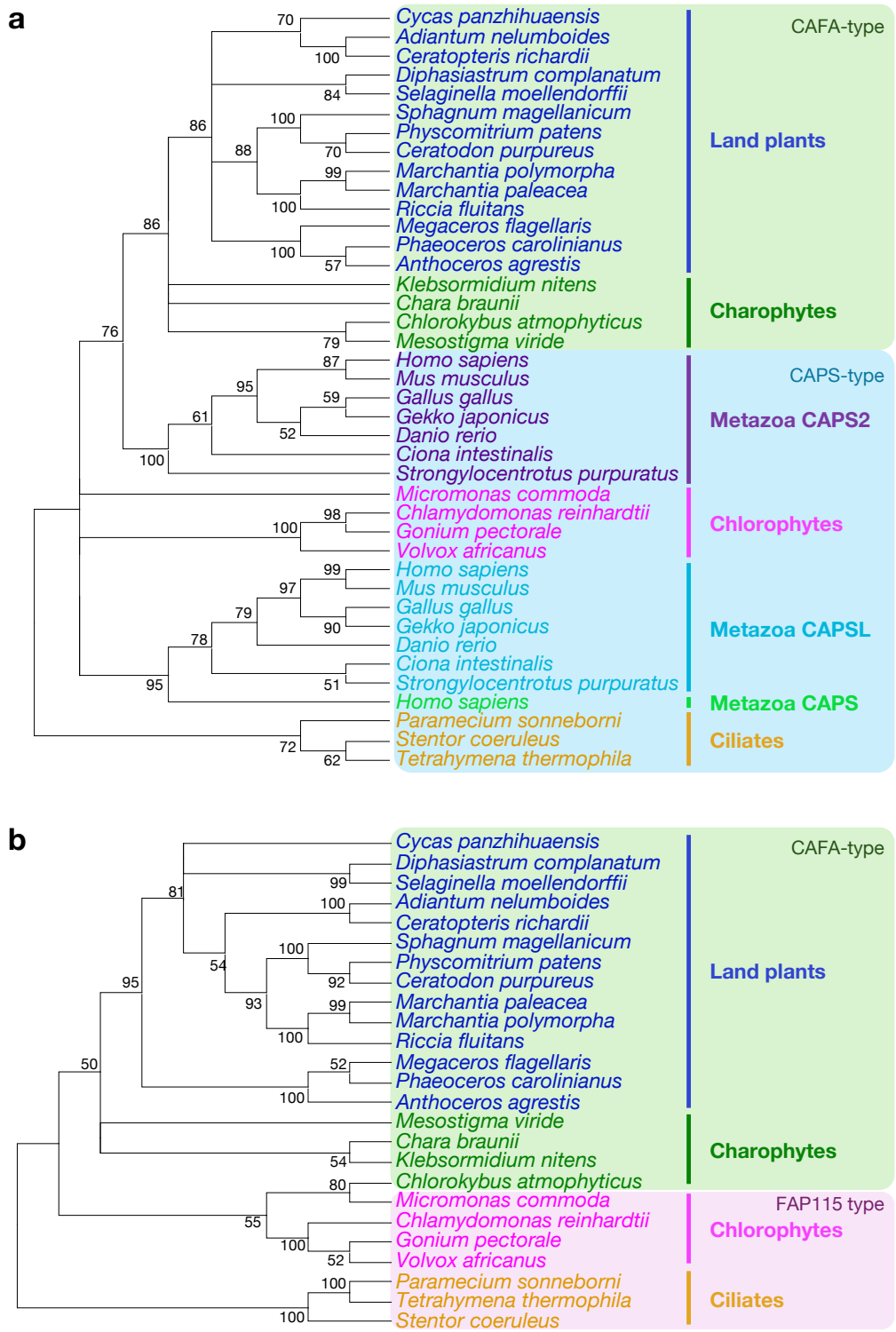

Fig. 2 Phylogenetic analyses of conserved CAPS- and FAP115-like domains

Phylogenetic trees of the CAPS-like (**a**) and FAP115-like (**b**) domains, respectively. Phylogenetic trees were inferred using NJ method with JTT model. Numbers at nodes indicate support values obtained with 1,000 bootstrap replicates using the MEGA11 software.

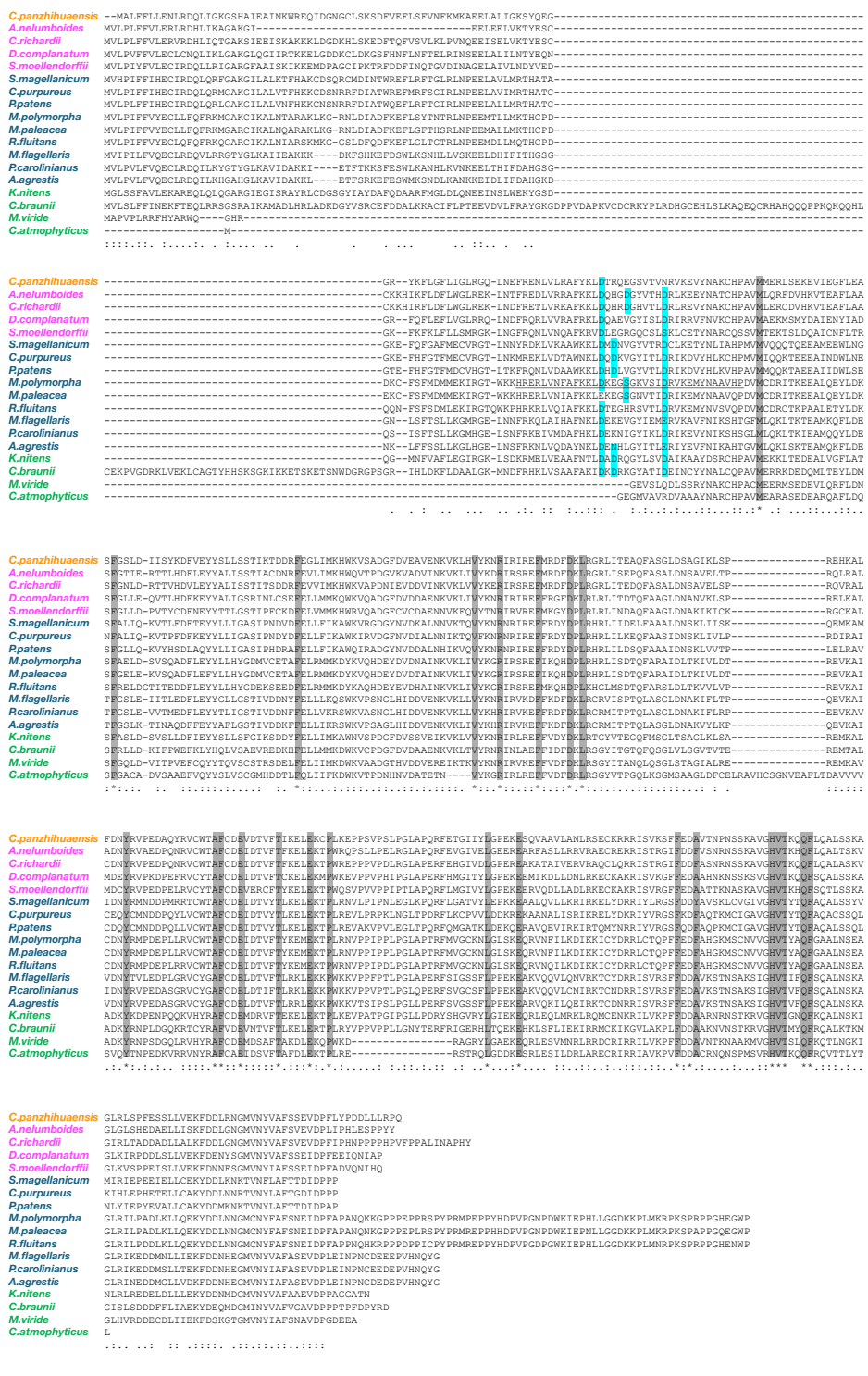

Fig. 3 Multiple sequence alignment of MpCAFA and its homologs

Gymnosperm, pteridophytes, bryophytes and charophytes are shown in orange, magenta, blue and green, respectively. EF-hand domain predicted by InterProScan in *M. polymorpha* is shown underlined, and amino acid residues predicted to be involved in calcium binding are highlighted in cyan. Amino acid residues conserved among the species shown here are highlighted in grey.

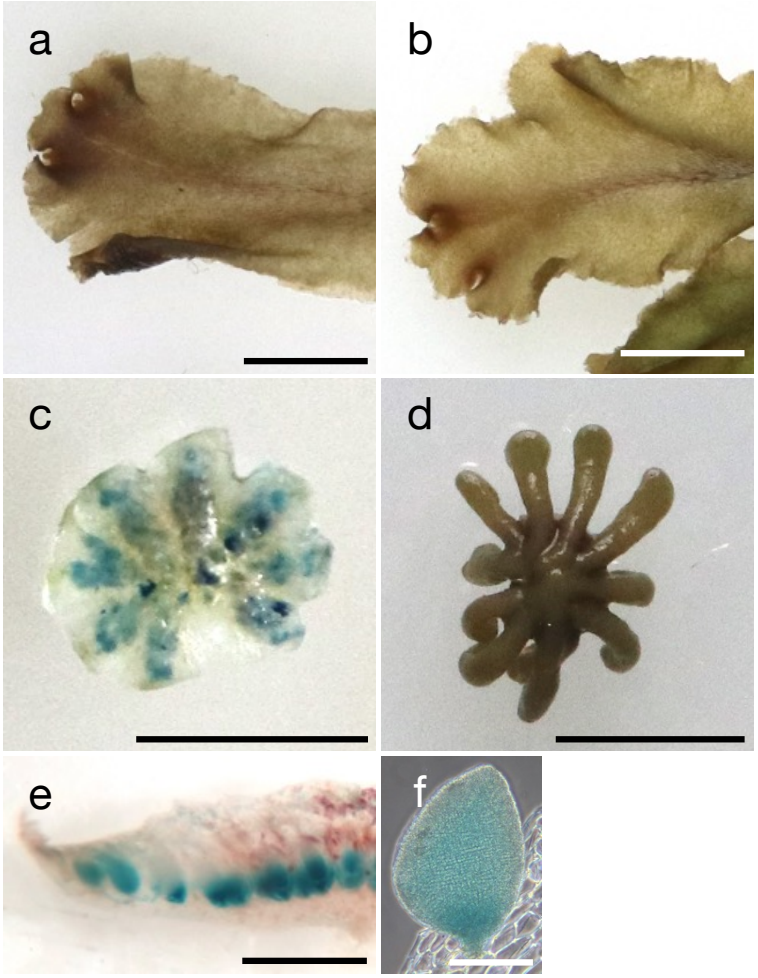

Fig. 4 Antheridium-specific expression of Mp*CAFA*

GUS staining of plants carrying the Mp$CAFA_{pro}$:*GUS* construct. Male (**a**) and female (**b**) thalli, antheridiophore (**c**), archegoniophore (**d**), longitudinal sections of male receptacle (**e**) and antheridium (**f**). Scale bars, 1 cm (**a** and **b**), 5 mm (**c** and **d**), 1 mm (**e**), and 250 µm (**f**).

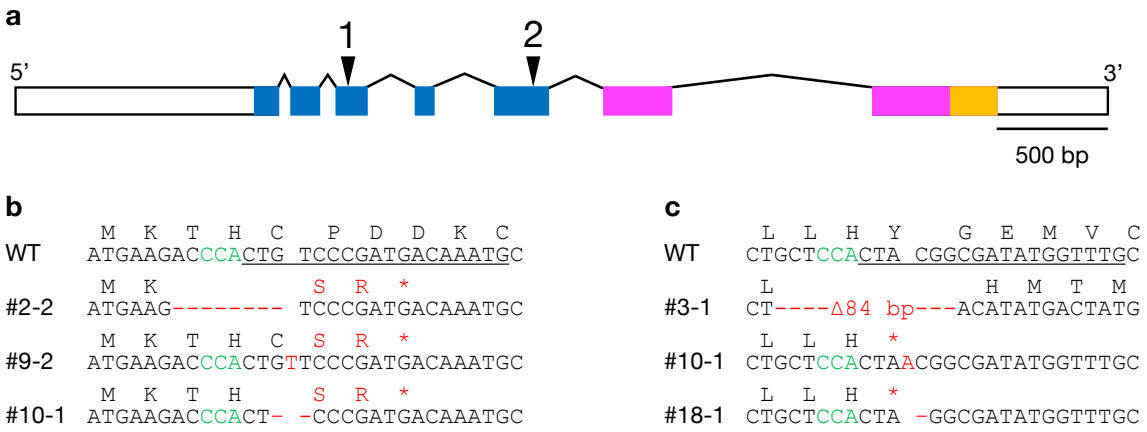

Fig. 5 Generation of male loss-of-function Mp*cafa*^{ge} mutants

(**a**) Schematic illustration of the Mp*CAFA* gene. Open and filled boxes indicate untranslated and coding regions, respectively. CAPS- and FAP115-like domains and PRD are shown in blue, magenta and orange, respectively. Triangles indicate the target sites for CRISPR/Cas9. (**b**) and (**c**) Mutations introduced by CRISPR/Cas9 at the target sites 1 and 2 in (**a**), respectively. Nucleotide sequences of the target sites in the wild-type (WT) and male mutants (*e.g.*, #2-2) are shown with translated amino acid sequence above for each. The target and PAM sequences are underlined and in green, respectively. Mutations are shown in red. Long deletion is indicated with the number of deleted nucleotides. Asterisks indicate translational stops introduced by genome-editing. Sequences in female mutants are given in Fig. S2.

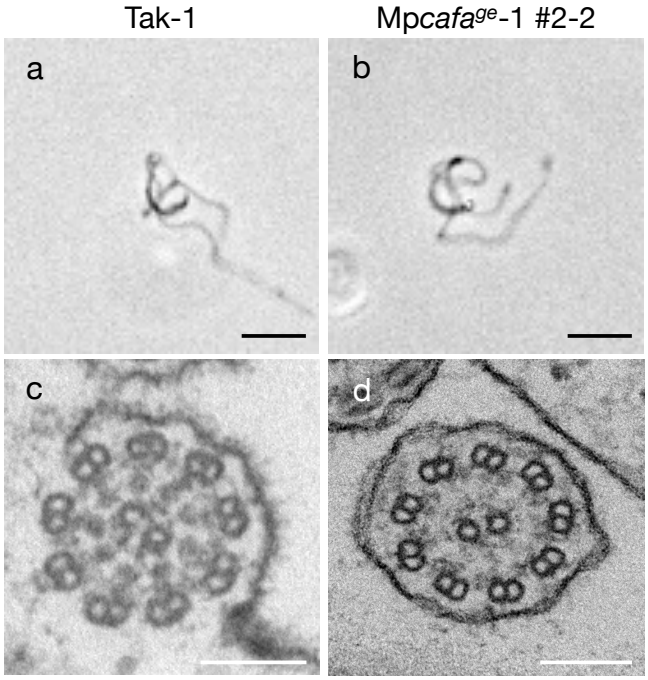

Fig. 6 Morphology and axoneme structure are normal in Mp*cafa*^{ge} spermatozoids

(**a**) and (**b**)**,** Phase-contrast images of spermatozoids from wild-type male, Tak-1, and representative Mp*cafa*^{ge}-1 #2-2, respectively. Scale bar, 10 µm. (**c**) and (**d**), TEM cross-sections of cilia from Tak-1 and Mp*cafa*^{ge} #2-2 spermatozoids, respectively. Scale bar, 100 nm.

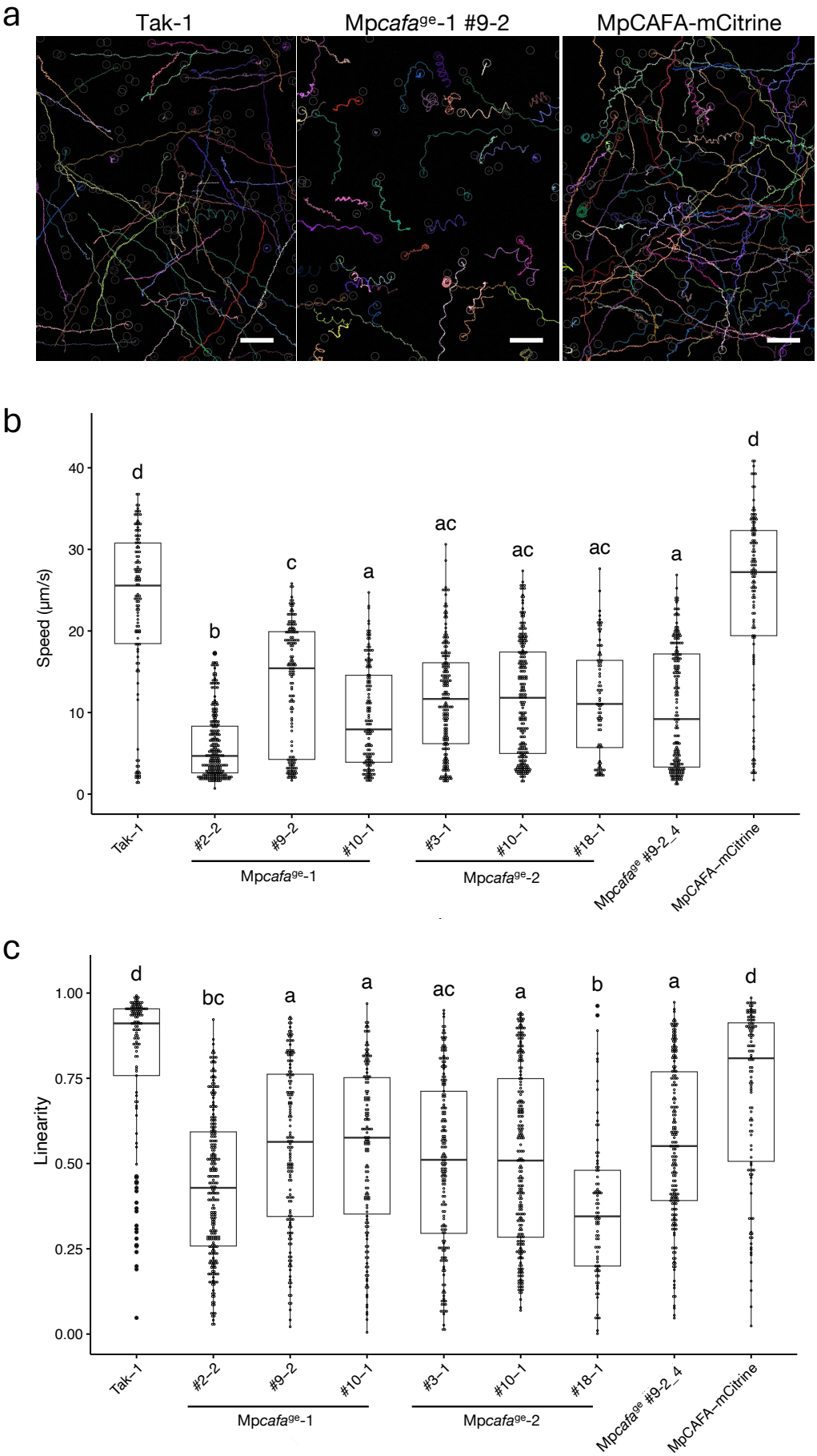
a
Tak-1
Mpcafa^ge-1 #9-2
MpCAFA-mCitrine
b
Speed (μm/s)
0
10
20
30
40
d
b
c
a
ac
ac
ac
a
d
Tak-1
#2-2
#9-2
#10-1
#3-1
#10-1
#18-1
Mpcafa^ge #9-2_4
MpCAFA-mCitrine
Mpcafa^ge-1
Mpcafa^ge-2
c
Linearity
0.00
0.25
0.50
0.75
1.00
d
bc
a
a
ac
a
b
a
d
Tak-1
#2-2
#9-2
#10-1
#3-1
#10-1
#18-1
Mpcafa^ge #9-2_4
MpCAFA-mCitrine
Mpcafa^ge-1
Mpcafa^ge-2

Fig. 7 Spermatozoid motility was impaired in Mp*cafa*^{ge} plants

(**a**) Trajectories of wild-type (Tak-1), representative mutant (Mp*cafa*^{ge}-1 #9-2) and complemented (Mp*cafa*^{ge} Mp*CAFA-mCitrine*) spermatozoids, respectively. Each spermatozoid was tracked for 10 seconds. Scale bar, 50 µm. (**b**) and (**c**) Box-and-whisker plots of spermatozoid swimming speed and linearity, respectively. Mp*cafa*^{ge} #9-2_4, one of progenies obtained by crossing Mp*cafa*^{ge} #9-2 with wild-type female and lacks the CRISPR/Cas9 construct. MpCAFA-mCitrine, Mp*cafa*^{ge} #9-2_4 plant carrying Mp$CAFA_{pro}$:Mp*CAFA-mCitrine.* The upper and lower limits indicate the first and third interquartile ranges, respectively, and the middle bars indicates the medians Whiskers indicate ±1.5× the interquartile ranges. Different lowercase letters indicate significant differences ($P < 0.05$; Tukey–Kramer test). n=121, 245, 149, 139, 177, 223, 83, 188 and 114 spermatozoids of Tak-1, Mp*cafa*^{ge}-1 #2-2, #9-2 and #10-1, Mp*cafa*^{ge}-2 #3-1, #10-1 and #18-1, and MpCAFA-mCitrine, respectively.

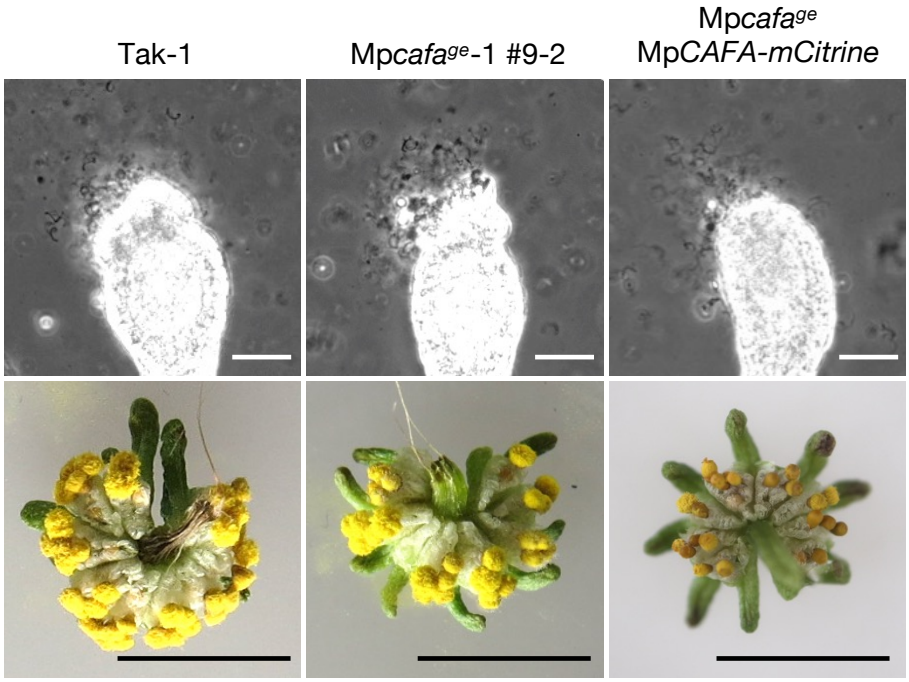

Fig. 8 Mp*cafa*^{ge} spermatozoids were attracted to an archegonium and fertile

Top, Attraction of wild-type, Mp*cafa*^{ge} and Mp*cafa*^{ge} Mp*CAFA-mCitrine* spermatozoids, to wild-type archegonia. Note that spermatozoids are attracted to the base of each archegonium, instead of the tip of the neck. Scale bar, 30 µm. **Bottom**, Spores formed by crossing wild-type, Mp*cafa*^{ge} and Mp*cafa*^{ge} Mp*CAFA-mCitrine* spermatozoids to wild-type female. Scale bar, 1 mm.

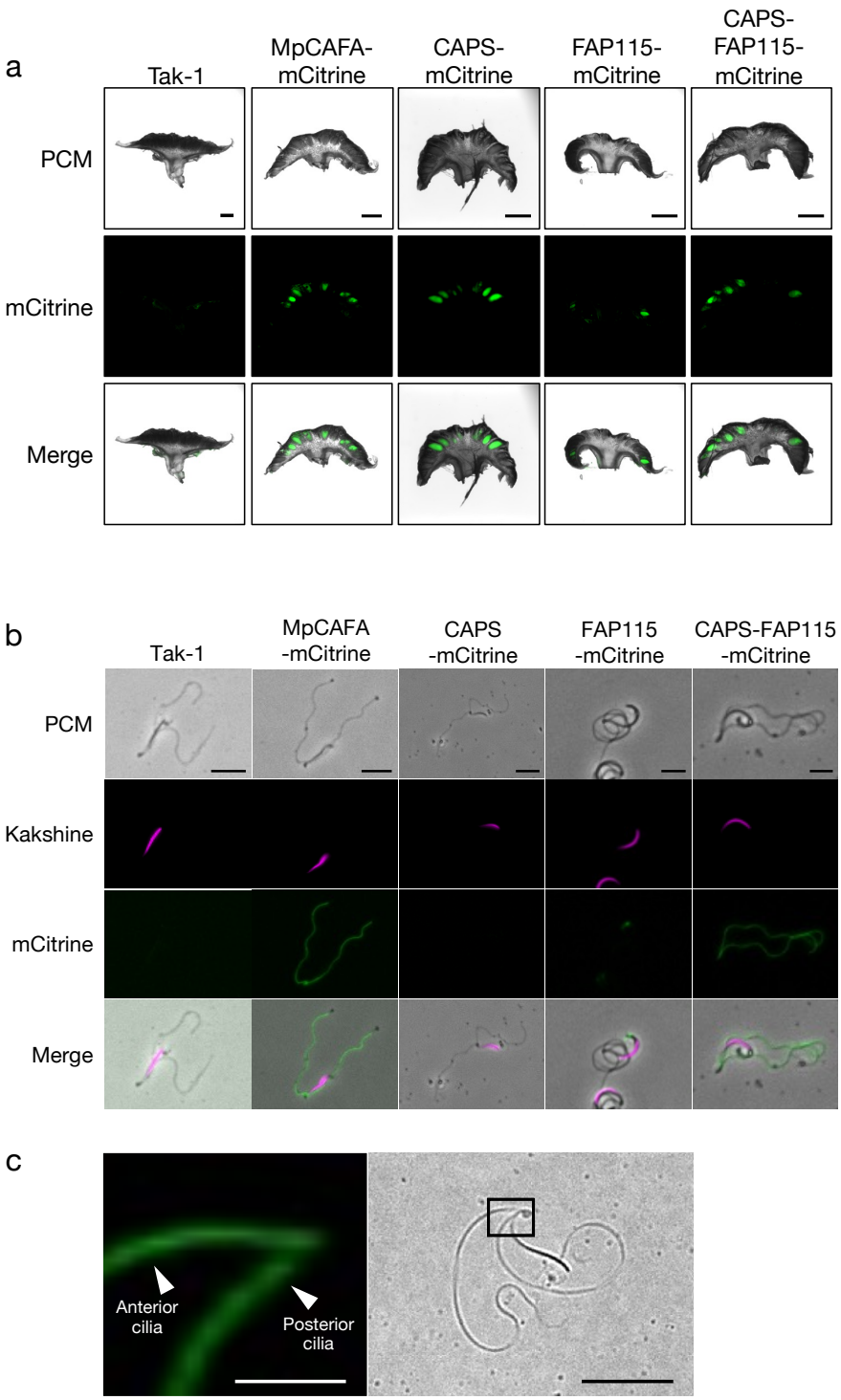

Fig. 9 Localization of MpCAFA and its truncated proteins

(**a**) and (**b**) Antheridiophores and spermatozoids from Mp*cafa*^{ge} plants expressing the constructs shown above, respectively. PCM, phase-contrast microscopy. Scale bar, 10 µm. (**c**) The basal ends of cilia expressing MpCAFA-mCitrine (left), enlarged from the boxed area in the right panel. Scale bars, 25 and 100 µm in the left and right panels, respectively. **c** Expression of mCitrine-tagged proteins in male receptacles. Scale bar, 1 mm.

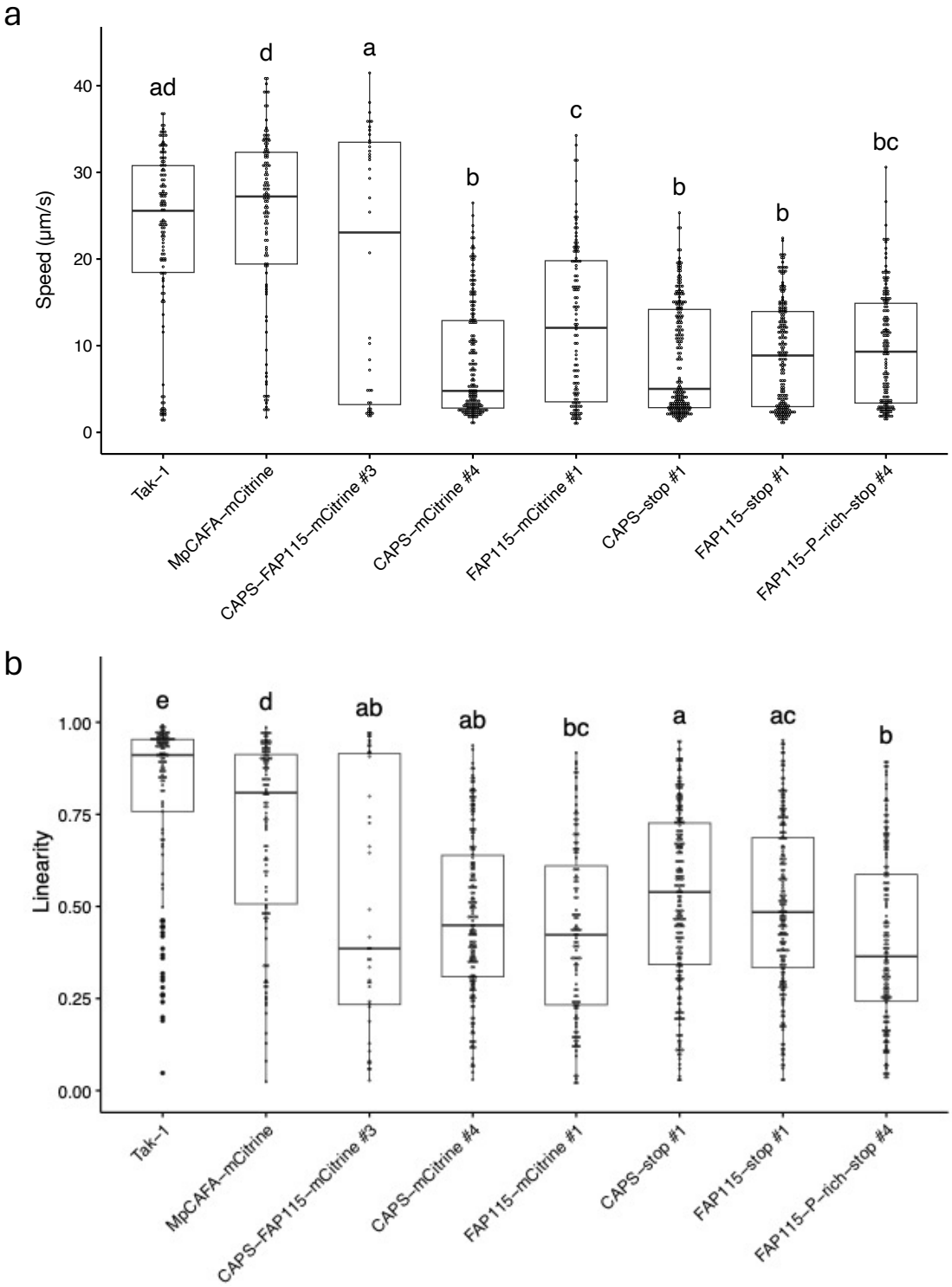

Fig. 10 Functional analysis of each domain of MpCAFA

Box-and-whisker plots of spermatozoid swimming speed (**a**) and linearity (**b**). The upper and lower limits indicate the first and third interquartile ranges, respectively, and the middle bars indicate the medians. Whiskers indicate ±1.5× the interquartile ranges. Different lowercase letters indicate significant differences ($P < 0.05$; Tukey–Kramer test). n=121, 114, 40, 178, 116, 216, 194 and 155 spermatozoids of Tak-1, MpCAFA-mCitrine,

CAPS-FAP115-mCitrine #3, CAPS-mCitrine #4, CAPS-stop #1, FAP115-mCitrine #1, FAP115-stop #1 and FAP115-P-rich-stop #4, respectively.

Supplementary tables

Table S1 List of primers used in this study

Table S2 List of amino acid sequences used for phylogenetic analysis

Legends for supplementary figures

Fig. S1 Vector construction

Schematic diagrams of constructs used in this study. Note that only Mp*CAFA*$_{pro}$-driven cassettes of the vectors are depicted. The backbone vector for each construct is given in parentheses. mC, mCitrine.

Fig. S2 Mutated sequences at the target sites in female Mp*cafa*^{ge} plants

(**a**) and (**b**) Mutations introduced by CRISPR/Cas9 at the target sites 1 and 2, respectively. Nucleotide sequences of the target sites in the wild-type (WT) and female mutants (*e.g.*, 4-3) are shown with translated amino acid sequence above for each. The target and PAM sequences are underlined and in green, respectively. Mutations are shown in red. Long deletion is indicated with the number of deleted nucleotides. Asterisks indicate translational stops introduced by genome-editing.

Fig. S3 Morphologies of Mp*cafa*^{ge} plants

Thalli grown from gemmae for 14 days and sexual organs of male (left) and female (right), respectively. Scale bars, 1 cm (Thalli).

Fig. S4 *CAFA*-like sequences in the *G. biloba* genome

Sequences similar to the Cycas CAFA (CYCAS_029556) found in the *G. biloba* genome (Liu et al. 2022). Only part of FAP115-like region was detected with multiple in-frame stop codons (indicated by asterisks).

Legends for supplementary movies

Movie S1

Spermatozoid motility in WT. This movie was captured at 100 fps and is shown in real time.

Movie S2

Spermatozoid motility in Mp*cafa*^{ge}-1 #9-2. This movie was captured at 100 fps and is shown in real time.

Movie S3

Spermatozoid motility in Mp*cafa*^{ge}-2 #3-1. This movie was captured at 100 fps and is shown in real time.

Movie S4

Spermatozoid motility in Mp*cafa*^{ge}-1 #9-2_4. This movie was captured at 100 fps and is shown in real time.

Movie S5

Spermatozoid motility in Mp*cafa*^{ge}-1 Mp*CAFA*$_{pro}$:Mp*CAFA-mCitrine*. This movie was captured at 100 fps and is shown in real time.

Movie S6

Motility of spermatozoids expressing MpCAFA-mCitrine under fluorescent microscope.